Fire Technology, 58, 3297–3316, 2022
© 2022 The Author(s)
Manufactured in The United States
https://doi.org/10.1007/s10694-022-01267-6

Correction to: Experimental Study of the Fire Dynamics in a Semi-enclosure Formed by Photovoltaic (PV) Installations on Flat Roof Constructions

*Jens Steemann Kristensen**, *School of Engineering, Edinburgh Fire Research Centre, University of Edinburgh, Edinburgh EH9 3JL, UK and Department of Civil Engineering, Technical University of Denmark (DTU), Brovej, 2800 Kongens Lyngby, Denmark*
Benjamin Jacobs, School of Engineering, Edinburgh Fire Research Centre, University of Edinburgh, Edinburgh EH9 3JL, UK
Grunde Jomaas, School of Engineering, Edinburgh Fire Research Centre, University of Edinburgh, Edinburgh EH9 3JL, UK and FRISSBE, ZAG – Slovenian National Building and Civil Engineering Institute, Dimičeva 12, 1000 Ljubljana, Slovenia

Published online: 2 June 2022

Correction to: Fire Technology 2022 The Author(s) Manufactured in The United States https://doi.org/10.1007/s10694-022-01228-z

In the PDF of this article, the formatting of Tables and figures were incorrect and should have been the following information. The original article PDF has now been corrected.

Table 1

Incorrect

Table 1
Material Overview of Layers in the Roof Construction (RC) Mock-Up

	RC-A	RC-B	RC-C
L1:	PVC-based Roofing membrane—1.5 mm		
L2:	CSB—22 mm	MW—50 mm	PIR/Alu—60 mm
L3:	Air—131.5 mm	PVC-based Roofing membrane—1.5 mm	
L4:		EPS – 80 mm	EPS – 70 mm
L5:	Calcium Silicate Board (CSB)—44 mm		

* Correspondence should be addressed to: Jens Steemann Kristensen, E-mail: J.Kristensen@ed.ac.uk

Correct

	RC-A	RC-B	RC-C
L1:	PVC-based Roofing membrane - 1.5 mm		
L2:	CSB - 22 mm	MW - 50 mm	PIR/Alu - 60 mm
L3:	Air - 131.5 mm	PVC-based Roofing membrane - 1.5 mm	
L4:		EPS – 80 mm	EPS – 70 mm
L5:	Calcium Silicate Board (CSB) - 44 mm		

Introduction, Fourth Paragraph

Incorrect The presence of PV arrays on a roof establishes a gap between the backside of the PV module and the top of the roof construction that can be considered a semi-enclosure, which introduces a significant change of the fire dynamics in the case of a fire. To prevent flame spread along flat roof constructions without a BAPV system, the roofing membrane or roofing system should be compliant with standards, such as the North American UL790 [23] or European EN 13,501–5 [24]. The PV modules are designed to be compliant with UL61730 [25] (previously UL1703 [26]) or IEC 61,730 [27, 28], which are almost similar and mainly focused on the electrical system and thus, reduction of ignition probability. UL 61,730 does, but IEC 61,730 does not, acknowledge that the PV module, as a physical object, modifies the fire dynamics, which is why a series of standard tests based on UL 790 [23] have been introduced. However, the standards are pass/fail tests where the specifications to the test setup are vague and thus permit interpretations. As a result, the outcomes of the tests are not necessarily independent of the test facility and the test personnel.

Correct The presence of PV arrays on a roof establishes a gap between the backside of the PV module and the top of the roof construction that can be considered a semi-enclosure, which introduces a significant change of the fire dynamics in the case of a fire. To prevent flame spread along flat roof constructions without a BAPV system, the roofing membrane or roofing system should be compliant with standards, such as the North American UL 790 [23] or European EN 13501–5 [24]. The PV modules are designed to be compliant with UL 61730 [25] (previously UL 1703 [26]) or IEC 61730 [27, 28], which are almost similar and mainly focused on the electrical system and thus, reduction of ignition probability. UL 61730 does, but IEC 61730 does not, acknowledge that the PV module, as a physical object, modifies the fire dynamics, which is why a series of standard tests based on UL 790 [23] have been introduced. However, the standards are pass/fail tests where the specifications to the test setup are vague and thus permit interpretations. As a result, the outcomes of the tests are not necessarily independent of the test facility and the test personnel.

Introduction, Fifth Paragraph

Incorrect The European Committee of Electrotechnical Standardization, CEN-ELEC, has published the test report CLC/TR 50,670 ‘External fire exposure to roofs in combination with photovoltaic (PV) arrays — Test method(s)’ [29]. In

this test method, a gas burner designed as a substitute to the wood wool basket from test method 1 in CEN/TS 1187 [30] by Currenta GmbH und Co. OHG [31] is installed in between the tested PV module and a non-combustible surface. The PV module should be inclined 30° with the lowest edge elevated 15 cm above the subjacent surface. The suggested method is deemed to be a test of the PV module when exposed to a flame, rather than the combination of a roof and a PV module. As such, it can be concluded that no test method considers the system behaviour between components, as the current methods are tests of individual components.

Correct The European Committee of Electrotechnical Standardization, CENELEC, has published the test report CLC/TR 50670 'External fire exposure to roofs in combination with photovoltaic (PV) arrays—Test method(s)' [29]. In this test method, a gas burner designed as a substitute to the wood wool basket from test method 1 in CEN/TS 1187 [30] by Currenta GmbH und Co. OHG [31] is installed in between the tested PV module and a non-combustible surface. The PV module should be inclined 30° with the lowest edge elevated 15 cm above the subjacent surface. The suggested method is deemed to be a test of the PV module when exposed to a flame, rather than the combination of a roof and a PV module. As such, it can be concluded that no test method considers the system behaviour between components, as the current methods are tests of individual components.

Introduction, Sixth Paragraph

Incorrect However, Cancelliere et al. [32] fitted a modified version of the CLC/TR 50,670 test set-up in combination with 0.375 m2 roofing membrane within the single burning item extraction hood in an attempt to classify the PV modules as a construction product (EN 13,813 [33]). Since their modified tests were a combination of two products interacting with each other, the test method is not deemed to test a single construction product, but rather the test of a system in a specific predefined geometry which does not represent a likely geometry. As such, the tested method aligns with UL 61,730 and is deemed to be a pass/fail-test.

Correct However, Cancelliere et al. [32] fitted a modified version of the CLC/TR 50670 test set-up in combination with 0.375 m^2 roofing membrane within the single burning item extraction hood in an attempt to classify the PV modules as a construction product (EN 13813 [33]). Since their modified tests were a combination of two products interacting with each other, the test method is not deemed to test a single construction product, but rather the test of a system in a specific predefined geometry which does not represent a likely geometry. As such, the tested method aligns with UL 61730 and is deemed to be a pass/fail-test.

Introduction Eight Paragraph

Incorrect In terms of large scale experiments, Backstrom et al. summarised the result from experiments conducted with modified versions of the US standard test

Experimental Study of the Fire Dynamics method for roofing materials UL790 [39], whereas Kristensen and Jomaas conducted a series of large-scale experiments to understand flame spread on flat roof constructions with BAPV systems [40].

Correct In terms of large scale experiments, Backstrom et al. summarised the result from experiments conducted with modified versions of the US standard test Experimental Study of the Fire Dynamics method for roofing materials UL 790 [39], whereas Kristensen and Jomaas conducted a series of large-scale experiments to understand flame spread on flat roof constructions with BAPV systems [40].

Introduction, Ninth Paragraph 8th Line

Incorrect Despinasse and Krueger developed a novel test procedure, wherein they applied a gas burner to either the front or back side of PV modules and defined burn-through within 15 min as a failure criteria [43].

Correct Despinasse and Krueger developed a novel test procedure, wherein they applied a gas burner to either the front or back side of PV modules and defined burn-through within 15 min as a failure criteria [43].

Introduction, 12th Paragraph

Incorrect Based on the above, the current study focuses on the importance of the following four parameters: (i) The type of panel acting as a vertical barrier above the initial fire; (ii) The gap height between the roof surface and the vertical barrier; (iii) The inclination of the vertical barrier; (iv) The material subjacent to the roofing membrane. It is assumed that one roofing membrane is representative for all roofing membranes used on the European marked, as they have passed the same test regime to comply with a given classification (herein the European EN 13,501–5, 'Fire classification of construction products and building elements—Part 5: Classification using data from external fire exposure to roofs tests', [24], BROOF(t4)).

Correct Based on the above, the current study focuses on the importance of the following four parameters: (i) The type of panel acting as a vertical barrier above the initial fire; (ii) The gap height between the roof surface and the vertical barrier; (iii) The inclination of the vertical barrier; (iv) The material subjacent to the roofing membrane. It is assumed that one roofing membrane is representative for all roofing membranes used on the European marked, as they have passed the same test regime to comply with a given classification (herein the European EN 13501–5, 'Fire classification of construction products and building elements—Part 5: Classification using data from external fire exposure to roofs tests', [24], BROOF(t4)).

Equation 1

Incorrect

$$\frac{\dot{q}''_f(H \pm r\,tan(\theta))^2}{\dot{Q}(1 \pm sin(\theta))} = a\left(\frac{r}{H \pm r\,tan(\theta)}\right)^b \tag{1}$$

where: $a = 0.074, b = -1.232$

Correct

$$\frac{\dot{q}''_f\left(H \pm r\,tan(\theta)\right)^2}{\dot{Q}\left(1 \pm sin(\theta)\right)} = a\left(\frac{r}{H \pm r\,tan(\theta)}\right)^b$$

where:

$$a = 0.074, \quad b = -1.232$$

Re-Radiation in Semi-Enclosures with PV Modules, Fourth Paragraph

Incorrect The significantly smaller values on the x-axis for the plots based on data by Ju et al. are caused by a lower ratio between the gap distance δHρ and the distance between the heat source and the nearest heat flux gauge (r). By comparing the left-hand side of the model by Tang et al. (Eq. 1) with the data by Kristensen and Ju, it is noticed that the experimental data are significantly lower than the model predictions (Figure 2). It is not possible to make any exact comparison between similar measurements by Tang and Kristensen or Ju, but for H 1/4 0:194 m; h 1/4 10_; r 1/4 0:2 m, the heat flux is estimated to _q00_ 5:3 kW = m^2 for Q_1/4 7 kW in the experiments by Ju et al. [12], whereas the heat flux is measured to_q00f_ 10 kW = m^2 for Q_ 1/4 6:73 kW;H 1/4 0:25 m; h 1/4 0_ at the same distance to the heat source in the experiments by Tang et al. [13]. This does not correspond with the overall trend in the three papers, where the upstream heat flux, at a similar distance, should increase as a function of a gap height reduction as well as an inclination increase from 0 to 10_. Additionally, the reduction of the heat release rate (HRR) should also lead to a reduced heat flux, hereupon all three parameters (h;H; r) in the experiment by Tang et al. should result in a heat flux smaller than the one measured by Ju et al.

Correct The significantly smaller values on the x-axis for the plots based on data by Ju et al. are caused by a lower ratio between the gap distance (H) and the distance between the heat source and the nearest heat flux gauge (r). By comparing the left-hand side of the model by Tang et al. (Eq. 1) with the data by Kristensen and Ju, it is noticed that the experimental data are significantly lower than the model predictions (Figure 2). It is not possible to make any exact comparison between similar measurements by Tang and Kristensen or Ju, but for $H = 0.194$ m, $\theta = 10°$, $r = 0.2$ m, the heat flux is estimated to $\dot{q}f \approx 5.3$ kW/m^2 for $\dot{Q} = 7$ kW in the experiments by Ju et al. [12], whereas the heat flux is measured to $q > f \approx 10$ kW/$m2$ for $\dot{Q} = 6.73$ kW, $H = 0.25$ m, $\theta = 0°$ at the same distance to the heat source in the experiments by Tang

et al. [13]. This does not correspond with the overall trend in the three papers, where the upstream heat flux, at a similar distance, should increase as a function of a gap height reduction as well as an inclination increase from 0° to 10°. Additionally, the reduction of the heat release rate (HRR) should also lead to a reduced heat flux, whereupon all three parameters (θ, H, r) in the experiment byTang et al. should result in a heat flux smaller than the one measured by Ju et al.

Figure 3

Incorrect

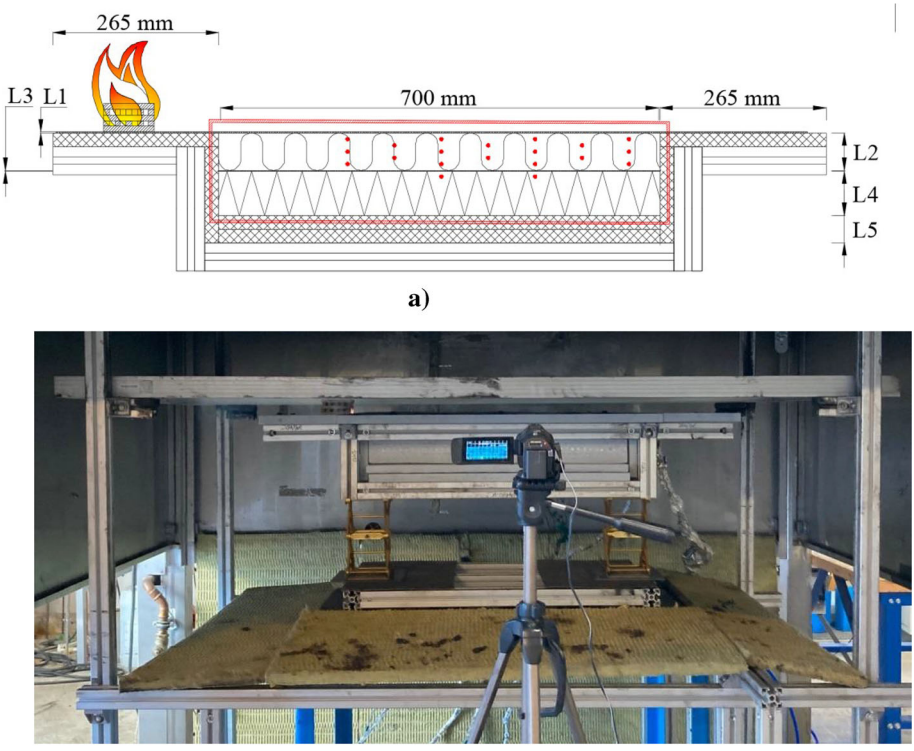

Figure 3. Visual overview of the experimental set-up. (a) Sketch of the mock-up used in the experiments. The roof construction mock-up is highlighted within the red square, where the thickness of the layers, L1 to L5, are in accordance with the roof construction types RC-B and RC-C as defined in Table 1. A total of 20 thermocouples (TCs) are marked with red dots. Four arrays of TCs (depth; 10 mm, 30 mm, 50 mm) were located at 50 mm, 200 mm, 350 mm, and 500 mm, and three TC sets (depths of 20 mm and 40 mm) were located at 125 mm, 275 mm, and 425 mm from the right side of the roof. Two additional TCs were installed in the EPS, at a depth of 70 mm below the two TC arrays located at 200 mm and 350 mm. (b) Side view of the experimental set-up with a horizsontal PV module installed with a gap height of 8 cm.

Correct

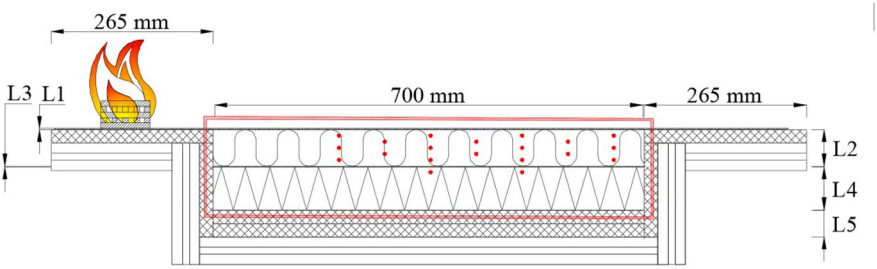

a) Sketch of the mock-up used in the experiments. The roof construction mock-up is highlighted within the red square, where the thickness of the layers, L1 to L5, are in accordance with the roof construction types RC-B and RC-C as defined in Table 1. A total of 20 thermocouples (TCs) are marked with red dots. Four arrays of TCs (depth; 10 mm, 30 mm, 50 mm) were located at 50 mm, 200 mm, 350 mm, and 500 mm, and three TC sets (depths of 20 mm and 40 mm) were located at 125 mm, 275 mm, and 425 mm from the right side of the roof. Two additional TCs were installed in the EPS, at a depth of 70 mm below the two TC arrays located at 200 mm and 350 mm.

b) Side view of the experimental set-up with a horizsontal PV module installed with a gap height of 8 cm

Figure 3. Visual overview of the experimental set-up.

Experimental Setup, Fourth Paragraph

Incorrect An experimental matrix (Table 2) was designed to obtain a gradual increase of material complexity. As such, the initial nine experiments (#1–#9) were designed to examine the existence of a critical gap height for the given set-up below a stainless- steel plate. In the next nine experiments (#10–#18), the subjacent calcium silicate board was replaced with mineral wool to understand the influence of the conductive heat transfer. Afterwards, in experiments #19–#31, the stainless-steel board was replaced with PV modules to determine its influence on the flame spread rate (FSR) and the heat transfer through the subjacent insulation

materials. The final examined parameter was the inclination of the modules, to examine the importance of the findings by Tang et al., who reported that a gradual increase of the inclination (up to 20°) cause an enhanced heat flux towards the upstream (see Figure 1) subjacent surface.

Correct An experimental matrix (Table 2) was designed to obtain a gradual increase of material complexity. As such, the initial nine experiments (#1–#9) were designed to examine the existence of a critical gap height for the given setup below a stainless-steel plate. In the next nine experiments (#10–#18), the subjacent calcium silicate board was replaced with mineral wool to understand the influence of the conductive heat transfer. Afterwards, in experiments #19–#31, the stainless-steel board was replaced with PV modules to determine its influence on the flame spread rate (FSR) and the heat transfer through the subjacent insulation materials. The final examined parameter was the inclination of the modules, to examine the importance of the findings by Tang et al., who reported that a gradual increase of the inclination (up to 20°) cause an enhanced heat flux towards the upstream (see Figure 1) subjacent surface.

Materials and Experimental Roof Mock-Up, First Paragraph

Incorrect A PVC-based roofing membrane, classified as BROOF(t4) in accordance with EN 13,501–5 (ENV 1187) when tested upon mineral wool or PIR insulation [24, 47, 48], was used for all the experiments. To mimic a larger roof construction and thus prevent shrinkage of the heated roofing membrane, the membrane was mechanically fastened on all four sides by 25 mm wide, thin, metal sheets and bolts connected to the aluminium profile system. The width of the upper layer of the membrane, L1, was 37 cm, whereas the width of all subjacent layers was limited by the 30 cm width of the mock-up box.

Correct A PVC-based roofing membrane, classified as BROOF(t4) in accordance with EN 13501–5 (ENV 1187) when tested upon mineral wool or PIR insulation [24, 47, 48], was used for all the experiments. To mimic a larger roof construction and thus prevent shrinkage of the heated roofing membrane, the membrane was mechanically fastened on all four sides by 25 mm wide, thin, metal sheets and bolts connected to the aluminium profile system. The width of the upper layer of the membrane, L1, was 37 cm, whereas the width of all subjacent layers was limited by the 30 cm width of the mock-up box.

Table 2

Incorrect

Table 2
Experimental Matrix with an Overview of the Panel Type, Roof Build-Up, Gap Height, and Inclination Used

Experiment	Panel type	Roof construction	Gap height, H (cm)	Inclination, θ
#1, #2:	SS	RC-A	8	0°
#3, #4, #5:			10	
#5, #6:			12	
#7, #8, #9:			11	
#10 #11:		RC-B	8	
#12, #13:			10	
#14, #15:			12	
#17, #18:			11	
#19:	PV1		12	
#20, #21:			11	
#22, #23:		RC-C		
#24, #25:		RC-B	10	
#26, #27:		RC-C		
#28, #29:		RC-B	8	
#30, #31:		RC-C		
#32, #33:		RC-B		10°
#34, #35:		RC-C		
#36:	PV2	RC-B		
#37:				13°
#38:				15°
#39:	PV3			10°
#40:			10	
#41:			11	
#42:			12	

SS stainless-steel board. PV1-PV3: PV module (Type defined in Table 4). Detailed description of the roof construction is found in Table 1 and Figure 3a. The gap height was defined at the location of ignition source and the inclination was defined from the horizontal surface of the roof mock-up

Correct

Experiment	Panel type	Roof construction	Gap height, H	Inclination, θ
#1, #2:	SS	RC-A	8 cm	0°
#3, #4, #5:			10 cm	
#5, #6:			12 cm	
#7, #8, #9:			11 cm	
#10 #11:		RC-B	8 cm	
#12, #13:			10 cm	
#14, #15:			12 cm	
#17, #18:			11 cm	
#19:	PV1		12 cm	
#20, #21:			11 cm	
#22, #23:		RC-C		
#24, #25:		RC-B	10 cm	
#26, #27:		RC-C		
#28, #29:		RC-B	8 cm	
#30, #31:		RC-C		
#32, #33:		RC-B		10°
#34, #35:		RC-C		
#36:	PV2	RC-B		
#37:				13°
#38:				15°
#39:	PV3			10°
#40:			10 cm	
#41:			11 cm	
#42:			12 cm	

Experimental matrix with an overview of the panel type, roof build-up, gap height, and inclination used. SS: stainless-steel board. PV1-PV3: PV module (Type defined in Table 4). Detailed description of the roof construction is found in Table 1 and Figure 3a. The gap height was defined at the location of ignition source and the inclination was defined from the horizontal surface of the roof mock-up.

Panels, First Paragraph

Incorrect Those conclusions align well with the back sheet only representing 2.8 to 3.5% of the module weight, whereas the encapsulate represents 6.3 to 8% [55]. The two highly thermally stable fluoropolymers Tedlar and Kynar are among the most used products for back sheets [55, 56] and with a heat of combustion between 4.1 kJ/g and 5.4 kJ/g [57], a very limited additional heat flux was expected.

Correct Those conclusions align well with the back sheet only representing 2.8–3.5% of the module weight, whereas the encapsulate represents 6.3–8% [55]. The two highly thermally stable fluoropolymers Tedlar and Kynar are among the most used products for back sheets [55,56] and with a heat of combustion between 4.1 and 5.4 kJ/g [57], a very limited additional heat flux was expected.

Table 4

Incorrect

Table 4
Brand, Physical Dimensions and Known Fire Related Certification of the PV Modules

PV#	Brand	Length [cm]	Width [cm]	Frame depth [cm]	Certification
PV1:	SUNTECH	195	99	4	Application Class A
PV2:	GCL Solar	164.5	99	2.8	NA
PV3:	AUO	156	104.6	3.9	TEC/EN 61215, IEC/EN 61730, Fire class C

Correct

Table 4
Brand, Physical Dimensions and Known Fire Related Certification of the PV Modules

PV#	Brand	Length [cm]	Width [cm]	Frame depth [cm]	Certification
PV1:	SUNTECH	195	99	4	Application Class A
PV2:	GCL Solar	164.5	99	2.8	NA
PV3:	AUO	156	104.6	3.9	TEC/EN 61215, IEC/EN 61730, Fire Class C

Figure 6

Incorrect

a)

b)

Figure 6. Backside of PV module (a) and top view of mock-up (b) for a gap height of 8 cm (Experiment 31). Flame spread occurred from left to right. (a) Backside of tested PV module. The dotted line illustrates the location and dimensions of the subjacent roofing membrane (37 cm times 118 cm). All plastics in the area directly above the roof mock-up have burned away and the light areas within the dotted square were transparent glass. Just outside the dotted square, the plastic had charred, whereas the rest of the PV module is sooted. (b) Top view of roof mock-up, where eight to nine PV cells delaminated from the backside of the PV module. The shaded area highlighted with a dotted white line marks the location and area of the wood crib used as ignition source.

Correct

a) Backside of tested PV module. The dotted line illustrates the location and dimensions of the subjacent roofing membrane (37 cm times 118 cm). All plastics in the area directly above the roof mock-up have burned away and the light areas within the dotted square were transparent glass. Just outside the dotted square, the plastic had charred, whereas the rest of the PV module is sooted.

b) Top view of roof mock-up, where eight to nine PV cells delaminated from the backside of the PV module. The shaded area highlighted with a dotted white line marks the location and area of the wood crib used as ignition source.

Figure 6. Backside of PV module (a) and top view of mock-up (b) for a gap height of 8 cm (Experiment 31). Flame spread occurred from left to right.

Figure 7

Incorrect

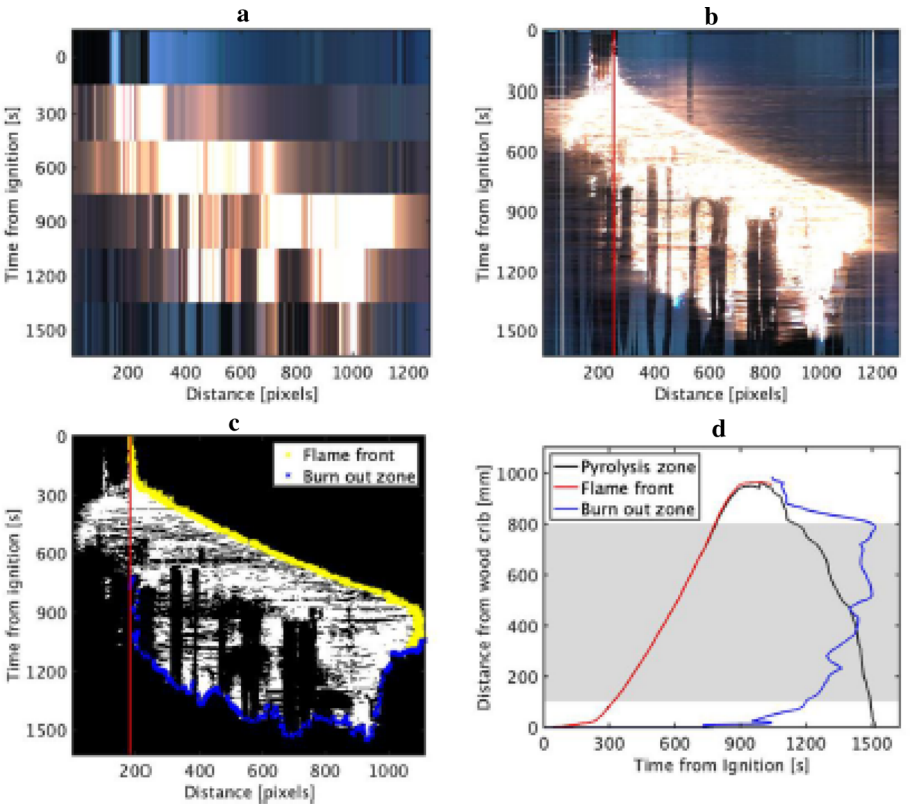

Figure 7. Visual overview of relevant steps in the single pixel line analysis process of experiment #25. Notice that time in represented on the y-axis in subplots a, b, and c. (a) Image of single pixel line for 300 s intervals equivalent to Figure 5a, b, d, f–h. (b) Intervals reduced to 1 s. Vertical white lines mark the ends of the roofing membrane, and the red line mark the right side of the wood crib. (c) Binary conversion of flame. Flame front and burn out zones identified. Notice that the distance is reduced to the width of the roofing membrane. (d) Plot of flame front and burn out location, as well as width of pyrolysis zone, as a function of time. The grey rectangle defines the location of the subjacent roof mock-up (see Figure 3). Note two things: (i) The black line defining the pyrolysis zone is covered by the red flame front line until the burn out zone detach from the wood crib after 700 s. (ii) The axes are switched compared to subplots a, b, and c.

Correct

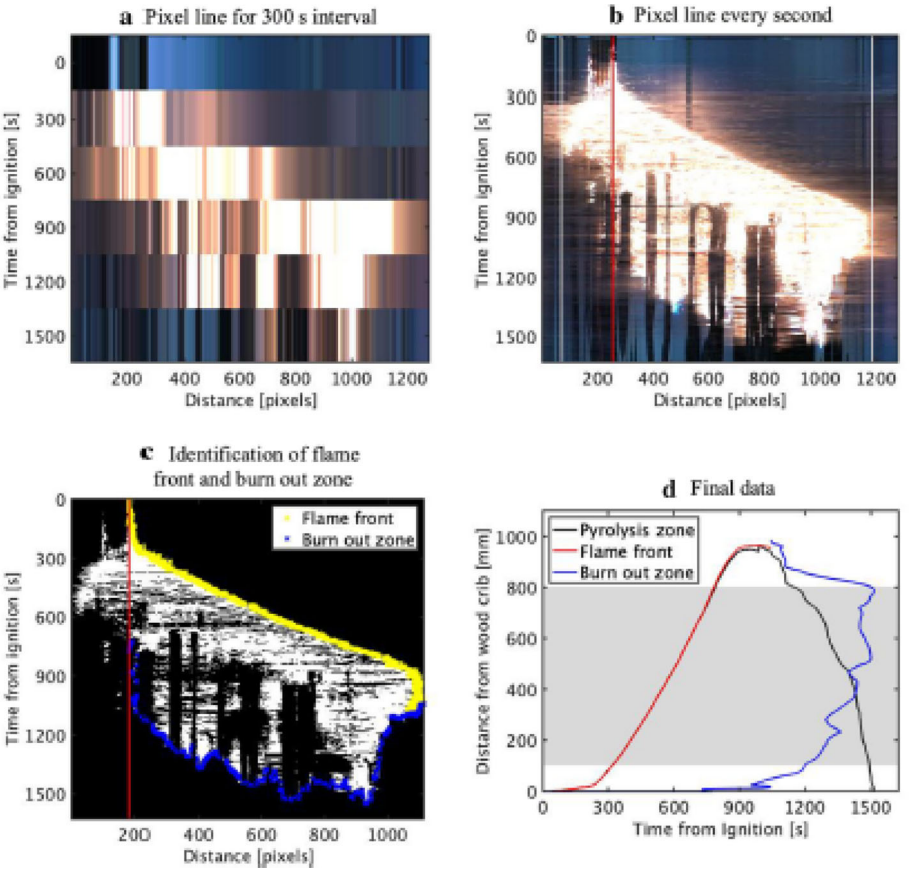

Figure 7. Visual overview of relevant steps in the single pixel line analysis process of experiment #25. Notice that time in represented on the y-axis in subplots a, b, and c. (a) Image of single pixel line for 300 s intervals equivalent to Figure 5a, b, d, f–h. (b) Intervals reduced to 1 s. Vertical white lines mark the ends of the roofing membrane, and the red line mark the right side of the wood crib. (c) Binary conversion of flame. Flame front and burn out zones identified. Notice that the distance is reduced to the width of the roofing membrane. (d) Plot of flame front and burn out location, as well as width of pyrolysis zone, as a function of time. The grey rectangle defines the location of the subjacent roof mock-up (see Figure 3). Note two things: (i) The black line defining the pyrolysis zone is covered by the red flame front line until the burn out zone detach from the wood crib after 700 s. (ii) The axes are switched compared to subplots a, b, and c.

Figure 8

Incorrect

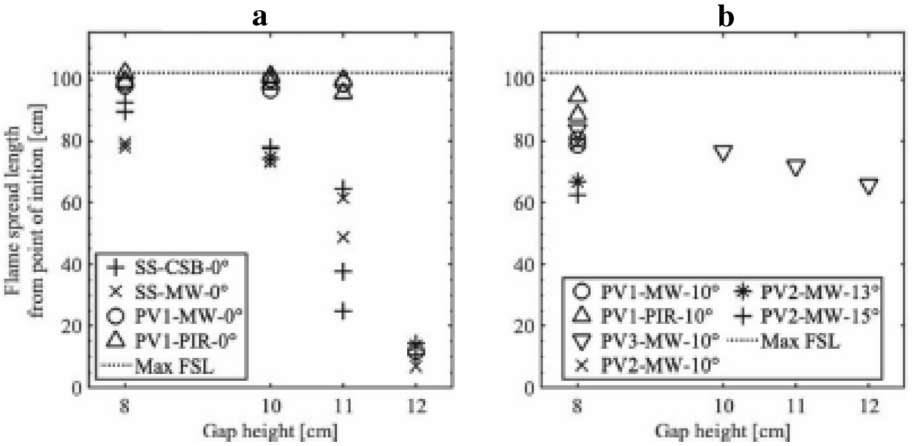

Figure 8. Flame spread length as a function of gap height, panel type (stainless-steel (SS) or PV module (PV1, PV2, PV3)), insulation material (calcium silica board (CSB), mineral wool (MW), or PIR insulation), and inclination of panel.

Correct

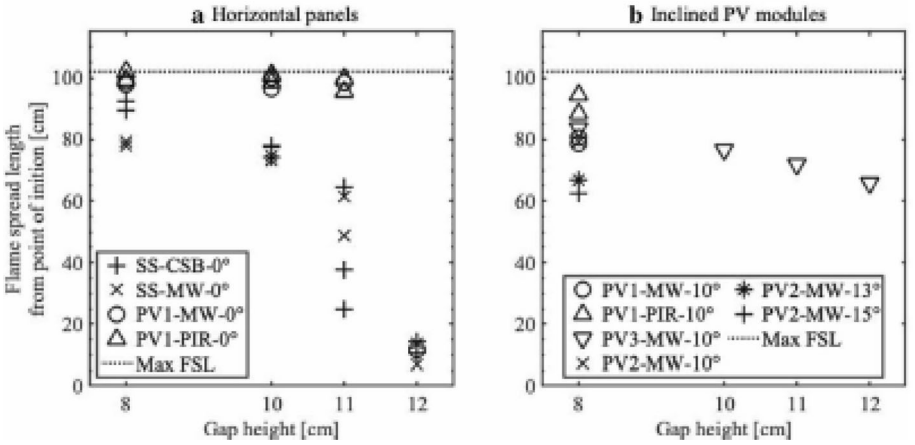

Figure 8. Flame spread length as a function of gap height, panel type (stainless-steel (SS) or PV module (PV1, PV2, PV3)), insulation material (calcium silica board (CSB), mineral wool (MW), or PIR insulation), and inclination of panel.

Flame Spread Length (FSL), Fourth, Fifth, Sixth Paragraph

Incorrect Based on the experiments conducted with inclined modules (Figure 8b), it was concluded that the critical gap height determined for horizontal modules did not represent the critical gap height for all inclinations, as the FSL for an inclination of 10° and a gap height of 12 cm exceeded the defined domain of the wood crib, xdom, significantly. This corresponds well with the concept of the model developed by Tang et al. (see Eq. 1), where it can be seen that the upstream heat flux, q_ 00 f, to a certain extent, will increase for positive inclinations, h, if the heat release rate (HRR), Q_, gap height, H, and distance to the heat source, r, are kept constant. As the HRR from the wood crib is assumed similar for all experiments, it can be concluded that the critical gap height is above 12 cm for PV modules at an inclination of 10°. The theory by Tang et al. [13] corresponds well with the visual observations from the experiments, as seen from the frames displayed in Figure 9. The photos show that the initial flame spread on the right side of the wood crib is significantly larger than flame spread to the left (at 300 s after ignition) (see Figure 9b). In comparison to the flame spread rate below a horizontal module (see Figure 5), the flame spread rate below an inclined PV module is significantly faster, as the FSL of around 80 cm is reached 570 s after ignition as opposed to 750 s below the horizontal PV module (Figure 5e).

However, none of the experiments with inclined modules reach the maximum obtained FSL as seen in the experiments conducted with horizontal PV modules (see Figure 8). For the given experimental set-up, an increased inclination, as well as increased gap height, cause a reduction of the FSL, as seen in Figure 9, where the flame front is stagnant between subfigures e and f. The results do not correlate well with the binary scenario below the horizontal modules, where the FSL was near the maximum length measured in the experiments with PV modules for a gap height of 11 cm or lower. From Figure 9e it is seen that the fire has detached from the source of ignition, but is unable to progress despite a wide pyrolysis zone that is assumed to entail a high heat release rate, as it is almost extinguished after 630 s (see Figure 9f). Based on Figure 8b, it can be concluded that it was a general trend that is linked to the experimental set-up rather than to the gap height and inclination.

Correct Based on the experiments conducted with inclined modules (Figure 8b), it was concluded that the critical gap height determined for horizontal modules did not represent the critical gap height for all inclinations, as the FSL for an inclination of 10° and a gap height of 12 cm exceeded the defined domain of the wood crib, *xdom*, significantly. This corresponds well with the concept of the model developed by Tang et al. (see Eq. 1), where it can be seen that the upstream heat flux, $\dot{q}''_f$, to a certain extent, will increase for positive inclinations, θ, if the heat release rate (HRR), $\dot{Q}$, gap height, H, and distance to the heat source, r, are kept constant. As the HRR from the wood crib is assumed similar for all experiments, it can be concluded that the critical gap height is above 12 cm for PV modules at an inclination of 10°. The theory by Tang et al. [13] corresponds well with the

visual observations from the experiments, as seen from the frames displayed in Figure 9. The photos show that the initial flame spread on the right side of the wood crib is significantly larger than flame spread to the left (at 300 s after ignition) (see Figure 9b). In comparison to the flame spread rate below a horizontal module (see Figure 5), the flame spread rate below an inclined PV module is significantly faster, as the FSL of around 80 cm is reached 570 s after ignition as opposed to 750 s below the horizontal PV module (Figure 5e).

However, none of the experiments with inclined modules reach the maximum obtained FSL as seen in the experiments conducted with horizontal PV modules (see Figure 8). For the given experimental set-up, an increased inclination, as well as increased gap height, cause a reduction of the FSL, as seen in Figure 9, where the flame front is stagnant between subfigures e and f. The results do not correlate well with the binary scenario below the horizontal modules, where the FSL was near the maximum length measured in the experiments with PV modules for a gap height of 11 cm or lower. From Figure 9e it is seen that the fire has detached from the source of ignition, but is unable to progress despite a wide pyrolysis zone that is assumed to entail a high heat release rate, as it is almost extinguished after 630 s (see Figure 9f). Based on Figure 8b, it can be concluded that it was a general trend that is linked to the experimental set-up rather than to the gap height and inclination.

Flame Spread Length (FSL), Last Paragraph

Incorrect Despite the limitations related to the sample width of the roofing membrane, the comparisons of FSL are deemed very relevant. Although the restricted sample width does not affect the ignition phase as the actual domain of the wood crib is significantly smaller than the width of the roofing membrane (see Figure 4). Thus,the definition of a critical gap height should not be based on the FSL, but solely on whether a specific set-up caused flame spread outside the domain of the ignition source. If that was the case, it should be assumed, that flame spread will occur below the full PV array, as seen in the large scale experiments [40]. Based on these findings, it can be concluded that the test set-up in the test method CLC/TR 50,670 [67] is not strict enough as self-sustained flame spread will occur for gap heights below 15 cm and inclinations below 30°.

Correct Despite the limitations related to the sample width of the roofing membrane, the comparisons of FSL are deemed very relevant. Although the restricted sample width does not affect the ignition phase as the actual domain of the wood crib is significantly smaller than the width of the roofing membrane (see Figure 4). Thus, the definition of a critical gap height should not be based on the FSL, but solely on whether a specific set-up caused flame spread outside the domain of the ignition source. If that was the case, it should be assumed, that flame spread will occur below the full PV array, as seen in the large scale experiments [40]. Based on these findings, it can be concluded that the test set-up in the test method CLC/TR 50670 [67] is not strict enough as self-sustained flame spread will occur for gap heights below 15 cm and inclinations below 30°.

Figure 9 Caption

Incorrect Figure 9 Side view of flame spread along a 118 cm long and 37 cm wide roofing membrane in an 8 cm gap between a horizontal roof construction mock-up and PV module with a 10º inclination (Experiment #32)

Correct Figure 9 Side view of flame spread along a 118 cm long and 37 cm wide roofing membrane in an 8 cm gap between a horizontal roof construction mock-up and PV module with a 10º inclination (Experiment #32).

Temperature

Purely based on the 0.014 W = m = K conductivity difference between the mineral wool and PIR insulation (Table 3), the temperature difference should increase with an enhanced depth. However, the trend seems to be different through a depth of 5 cm (see Figure 13c–e), which might be related to the conductivity being temperature dependent, and the physical changes of the PIR insulation. Although the conductivities at high temperatures is not tested for construction products, it is known that mineral wool products used in industry have a conductivity of around 0.12 W = m = K when heated to 500 ℃ [71]. On the other hand, the behaviour of the PIR insulation was complex. The conductivity at high temperatures is unknown, but the thickness increased when the material was heated, and mass loss was observed due to thermal degradation. Based on those findings, the relevance of the conductivities, reported in the product data sheets (Table 3), can be questioned in case of fire as they are not representative for high temperature cases.

The influence of the insulation thickness was evident when looking at the maximum temperatures recorded in the EPS insulation at a depth of 70 mm (Figure 13f). With the mineral wool having a thickness of 50 mm, the upper surface of the subjacent EPS was exposed to temperatures of minimum 250℃ (Figure 13e), which exceeded the melting temperature of EPS (100℃) [72].

Correct Purely based on the 0.014 $Wm^{-1}K^{-1}$ conductivity difference between the mineral wool and PIR insulation (Table 3), the temperature difference should increase with an enhanced depth. However, the trend seems to be different through a depth of 5 cm (see Figure 13c–e), which might be related to the conductivity being temperature dependent, and the physical changes of the PIR insulation. Although the conductivities at high temperatures is not tested for construction products, it is known that mineral wool products used in industry have a conductivity of around 0.12 $Wm^{-1}K^{-1}$ when heated to 500 ℃ [71]. On the other hand, the behaviour of the PIR insulation was complex. The conductivity at high temperatures is unknown, but the thickness increased when the material was heated, and mass loss was observed due to thermal degradation. Based on those findings, the relevance of the conductivities, reported in the product data sheets (Table 3), can be questioned in case of fire as they are not representative for high temperature cases.

The influence of the insulation thickness was evident when looking at the maximum temperatures recorded in the EPS insulation at a depth of 70 mm (Figure 13f). With the mineral wool having a thickness of 50 mm, the upper surface of the subjacent EPS was exposed to temperatures of minimum 250 ℃ (Figure 13e), which exceeded the melting temperature of EPS (100 ℃) [72].

IN Acknowledgements and Funding

Correct The authors would like to thank Ingka Services AB (formerly IKEA Services AB), ROCKWOOL International A/S and Kingspan Holdings (Irl) Limited for the financial support of the PhD project of Jens Steemann Kristensen.

Open Access

This article is licensed under a Creative Commons Attribution 4.0 International License, which permits use, sharing, adaptation, distribution and reproduction in any medium or format, as long as you give appropriate credit to the original author(s) and the source, provide a link to the Creative Commons licence, and indicate if changes were made. The images or other third party material in this article are included in the article's Creative Commons licence, unless indicated otherwise in a credit line to the material. If material is not included in the article's Creative Commons licence and your intended use is not permitted by statutory regulation or exceeds the permitted use, you will need to obtain permission directly from the copyright holder. To view a copy of this licence, visit http://creativecommons.org/licenses/by/4.0/.

Publisher's note Springer Nature remains neutral with regard to jurisdictional claims in published maps and institutional affiliations.